

PACS numbers: 42.55.Rz; 42.55.Xi; 42.60.Lh
DOI: 10.1070/QE2006v036n04ABEH013140

Devoted to the memory of Lev Petrovich Feoktistov

Efficiency of resonance pumping and optical gain in a Nd-doped phosphate glass excited by diode arrays

A.P. Bogatov, A.E. Drakin, G.T. Mikaelyan, D.R. Miftakhutdinov, V.I. Stadnichuk, A.N. Starodub

***Abstract*. The gain $\sim 3.5 \times 10^{-3}$ cm^{-1} is obtained in the repetitively pulsed regime upon pumping a Nd-doped phosphate glass into the $^4I_{9/2} - {}^4F_{3/2}$ absorption band by diode arrays at 874 nm. The pump efficiency for a sample of volume 6.7 cm^3 exceeded 0.5 and was limited only by the geometrical factor and the excited-state lifetime of the Nd^{3+} ion.**

Keywords: *diode pumping, Nd-doped phosphate glass, repetitively pulsed regime, resonance transition.*

1. Introduction

At present one of the promising applications of diode lasers (heterolasers) is their use for optical pumping high-power solid-state lasers. This is explained to a great extent by a high total efficiency of heterolasers (above 50 %) operating under comparatively simple conditions, in particular, at the nearly room temperature of a heat sink, which became possible recently. Optical pumping of solid-state lasers by diode lasers has been used already for more than 30 years and it is now widely employed in commercial devices. Modern advances in the field of diode-pumped solid-state lasers are comprehensively described in review [1]. The earlier papers on the diode pumping of neodymium-doped media were mainly devoted to crystals. This is explained by the fact that the stimulated transition cross section in a crystal matrix is almost an order of magnitude higher than that in a glass matrix. As a result, the threshold pump power for Nd^{3+} ions in a crystal matrix is considerably lower and, therefore, the required number of diode lasers is smaller. However, for the development of a high-power laser or an amplifier with a high stored energy ($\gtrsim 100$ J) a high cross section is no longer an advantage but a disadvantage, which was pointed out in [2]. The reason is a considerable extraction of the stored energy by the amplified spontaneous radiation and a low density of the saturation energy. Because of this, along with the development of new types of active media, the use of Nd^{3+}-doped glass matrices in diode-pumped high-power lasers remains to be of current interest.

Here, it is pertinent to mention new advances in the development of laser technology achieved in the last years (see, for example, papers [3 – 8] where the fabrication of high-power solid-state lasers was reported). The obvious and well-known advantage of a diode-pumped solid-state laser over a similar flashlamp-pumped laser is its much higher total (from a socket) efficiency. One should bear in mind that it is important that not only the energy losses in the laser are lower and the energy is saved, but also that these reduced losses weakly heat an active element. The latter circumstance is the most important in most cases because it alleviates the requirements to the heat conduction of a material and cooling systems, improves the quality of the optical beam and the reliability and service life of the laser as whole.

Diode lasers used for pumping should have a number of special properties. The power of an individual diode laser (single-element heterolaser) is limited and achieves at present a few watts (~ 20 W in the best case). Therefore, the efficient pump system should contain no less than a few hundreds, and in reality, a few thousands of heterolaser chips. It is obvious that such a system can be realised only when individual laser chips are integrated in a standard composed radiation source containing tens or hundreds of laser chips. The design of such a composed radiation source, for example, in the form of a bar or a two-dimensional array should be optimised taking into account the optical and spectroscopic parameters of a medium being pumped. It was found that even the shape of a solid-state active element (rod, slab or disc) requires the corresponding optimisation of such a composed radiation source. This was pointed out, for example, in paper [9], where the requirements to the average brightness of the beam of a composed radiation source were formulated depending on the active-element shape. The above discussion shows that the concept of using diode pumping for high-power solid-state lasers poses a number of new scientific problems whose solution will determine the quality of the developed lasers and the scope of their applications.

Because the development of a high-power solid-state laser requires considerable material expenses, the technical elaboration of the laser should be preceded by its simulation. This paper belongs to this direction of studies. The reliable simulation can be performed when the accurate data on the optical and spectral parameters of the active element

A.P. Bogatov, A.E. Drakin, , D.R. Miftakhutdinov, V.I. Stadnichuk, A.N. Starodub P.N. Lebedev Physics Institute, Russian Academy of Sciences, Leninsky prosp. 53, 119991 Moscow, Russia; e-mail: bogatov@sci.lebedev.ru;
G.T. Mikaelyan Federal State Unitary Enterprise, Inject Research and Production Association, prosp. 50 let Oktyabrya 101, 410052 Saratov, Russia; e-mail: inject@overta.ru

Received 28 December 2005; revision received 13 March 2006
Kvantovaya Elektronika **36** (4) 302 – 308 (2006)
Translated by M.N. Sapozhnikov

are available and adequate simulation methods are used. Note that despite the fact that numerous data on the parameters of active media are available at present, it is difficult to use them in simulations. It is more expedient to employ the data related to a particular sample under study. This also concerns our paper because we were not sure that the glass sample used in our study was identical with the required accuracy to the samples whose parameters were presented in handbooks or earlier papers. In addition, diode pumping requires a high accuracy of simulations because in this case the excess losses are absolutely inadmissible upon conversion of the beam energy of heterolasers to the beam energy of a solid-state laser. For this reason, we studied in this paper, in particular, the optical and spectral properties of the diode-pumped Nd-doped phosphate glass under the conditions close to those for high-power lasers.

These conditions assume, first, transverse pumping with a considerable penetration depth ($\sim 2-4$ cm), which should correspond to the aperture of the optical beam from a high-power laser or amplifier. Second, pumping should be performed with two-dimensional heterolaser arrays to provide a sufficiently high degree of integration of individual heterolaser chips. The Nd^{3+} ions were pumped resonantly into the 874-nm absorption band corresponding to the $^4I_{9/2} - {}^4F_{3/2}$ transition. Hereafter, the term 'resonance pumping' is used in accordance with the classical term 'resonance absorption' (emission), which occurs upon transitions between the ground and the first excited state of an atom or an ion. Resonance pumping reduces the heat release in the active element more than by a factor of 1.5, which is especially important in our case. Such pumping was earlier used for crystals (see, for example, [10–12]).

The aim of our paper was to obtain experimental data on the diode pumping of a Nd^{3+}-doped phosphate glass and to verify the method of simulation of its laser parameters for using these data for the development of high-power lasers. The phosphate glass was selected as an active medium because it possesses the best laser characteristics.

2. Experiment

2.1 Experimental method

The scheme of the main part of the experimental setup is presented in Fig. 1a. Active element (*1*) was a glass slab of cross section 1×0.5 cm and length 13.4 cm made of a GLS-22 glass. The ends of this slab were cut at the Brewster angle. The active element was pumped by radiation from four diode arrays (*2–5*) through prisms (Fig. 1b). The arrays were a two-dimensional group (35×21) of AlGaAs/GaAs heterolasers with a quantum-well active region and the total area of 0.5×1 cm. The arrays were fed with specially designed four-channel pulsed power supply (*15*), which produced rectangular current pulses of duration variable from 100 to 500 μs with a pulse repetition rate of 10–100 Hz. The amplitude of these pulses could be varied independently in each channel from 0 to 40 A.

The diagnostics of optical amplification produced in the active element was performed with special probe cw quantum-well InGaAs/AlGaAs/GaAs heterolaser (*8*) emitting at 1055 nm. The pump current of the laser was controlled with special power supply (*9*). The required quality of the optical beam from this laser was provided with the help of collimating lens (*7*) and aperture (*6*) of diameter ~ 3 mm. The laser beam passed through the central part of active element (*1*), apertures (*10*) (used as spatial filters) and was incident on photodetector (*12*) or spectrometer (*13*) based on an MDR-4 monochromator. Spatial optical filtration in front of photodetector (*12*) provided the suppression of a luminescence signal appearing in active element (*1*) upon its pumping down to the level not exceeding 0.05 of the addition to the signal from the probe laser due to its amplification after passage through element (*1*). The output signals from photodetector (*12*) and spectrometer (*13*) were fed to the inputs of a UNIPAN 232B lock-in amplifier and a Tektronix TDS-2022 oscilloscope. The preliminary processed output signals from the oscilloscope were transmitted as data files to control PC (*14*), to which the output signal of the amplifier was also fed. This computer also controlled the step motor of the spectrometer, allowing the automatic digital data processing.

The scheme of optical pumping of an active element is presented in more detail in Fig. 1b. A specific feature of the scheme is the inclined coupling of radiation at an angle of $\sim 40.5^\circ$ with respect to the normal to the side surface of the active element. This was performed with the help of special prisms glued with optical cement on broad (1 cm) side surfaces of the active element. The end surfaces of the prisms facing the array were covered with AR coatings. The side surfaces of the prisms were polished. Radiation from arrays at ~ 874 nm was coupled to the prism through its end face and then to the active element, which also had polished side surfaces. The prism inclination angle was selected so that the pump radiation inside the active element was within the angle of the total internal reflection on its side surfaces. The angles lying in the plane of incidence of the axial beam (plane of Fig. 1b) were most critical for the fulfilment of conditions of the total internal reflection. Because of this, chips were assembled on the array structure so that the 'slow' axis of the radiation pattern of a heterolaser (direction along the p–n transition in which the divergence is minimal) lied precisely in the plane of incidence.

The geometry of optical pumping used in this paper is a hybrid of the transverse pumping, when radiation is coupled through side surfaces, and longitudinal coupling at which the pump beam propagates, on the average, along the laser optical axis. Such a scheme combines the advantages of transverse pumping providing the possibility of using several radiation sources and of longitudinal pumping at which the efficiency of their use is maximal due to pumping over a considerable length.

Figure 1c shows the scheme for measuring the luminescence lifetime and spectra. Luminescence was detected perpendicular to the pump-beam direction. The sample thickness along the direction of luminescence detection was 0.5 cm, which excluded completely the possibility of radiation trapping because this thickness corresponded to the optically thin layer. Luminescence was excited both at ~ 874 and 800 nm. The detecting system was calibrated in the range from 700 to 1400 nm by using a TRSh 2850-3000 tungsten lamp and tabulated data on the radiating capacity of tungsten at temperature 2850°C.

2.2 Parameters of the active element

Although the typical characteristics of a GLS-22 glass are well known at present, for the reasons mentioned above, we measured the absorption and luminescence spectra and also

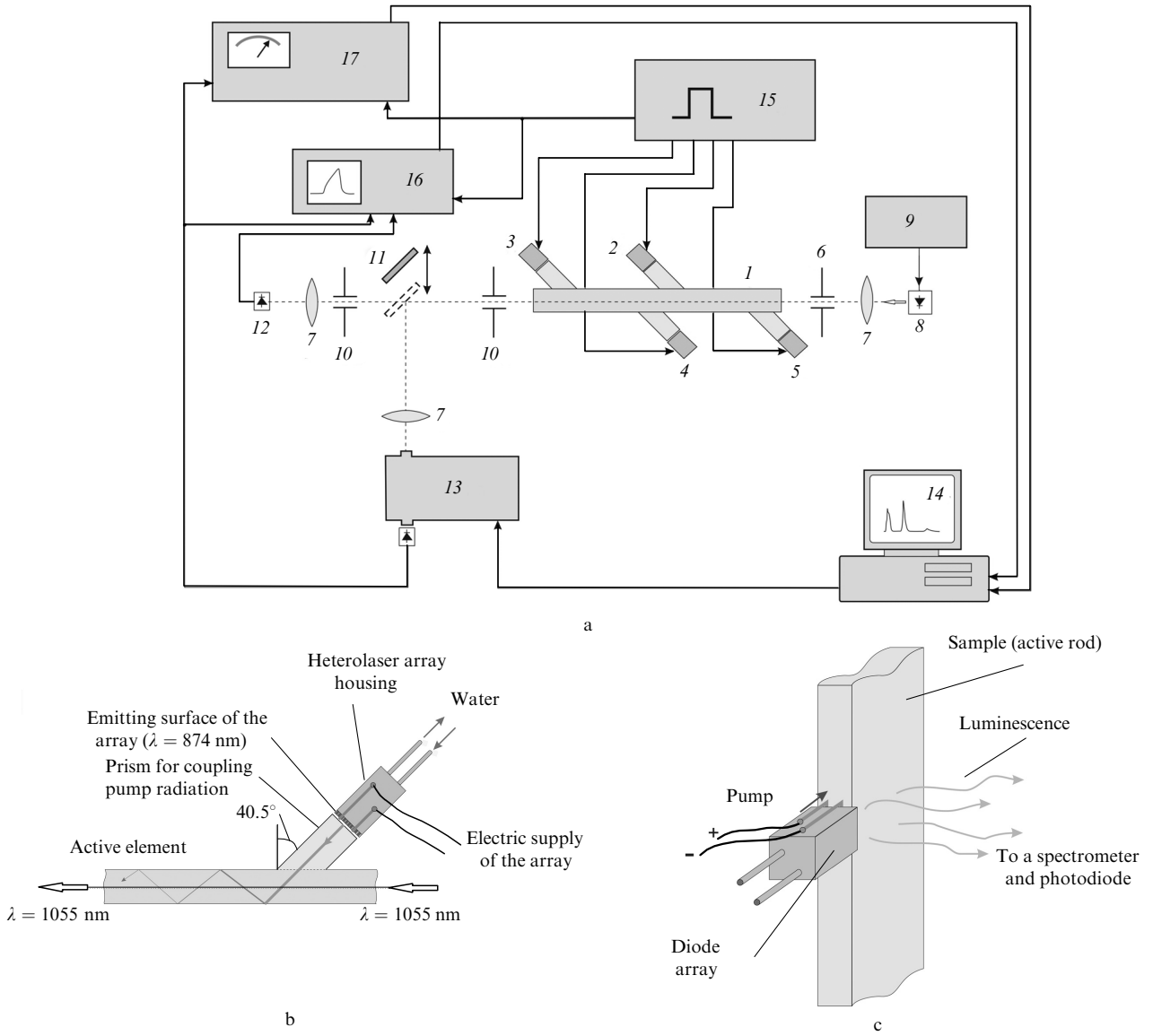

Figure 1. Block diagram of the setup for studying the optical and spectral characteristics of the active element (a); scheme for optical pumping an Nd-doped phosphate glass slab by radiation from a diode array (b); and scheme for studying luminescence (c): (*1*) active element; (*2–5*) diode arrays with prisms for coupling radiation into the active element; (*6*, *10*) apertures; (*7*) lenses; (*8*) probe 1055-nm laser; (*9*) current supply; (*11*) movable mirror; (*12*) photodiode; (*13*) spectrometer; (*14*) control computer; (*15*) power supply for diode arrays; (*16*) Tektronix TDS-2022 digital oscilloscope; (*17*) UNIPAN 232B selective nanovoltmeter.

the lifetime of the excited $^4F_{3/2}$ state for the active element under study.

These measurements were also motivated by the well-known fact that these characteristics can be sensitive to the spectral width of exciting radiation (see paper [13] and references therein).

Figure 2 shows the absorption spectrum of the active element. The measurement accuracy of the absorption coefficient was $\sim 2 \times 10^{-1}$ cm^{-1} at maxima and 2×10^{-2} cm^{-1} in the transparency region. The spectral resolution and measurement error of the wavelength were ~ 1 nm. The two bands at 801 and 874 nm in Fig. 2 correspond to the $^4I_{9/2} - {}^4F_{5/2}$ and $^4I_{9/2} - {}^4F_{3/2}$ transitions in the Nd^{3+} ion shown in the inset. One can see that the 801-nm absorption band has a smaller width compared to that of the 874-nm band and a considerably higher absorption coefficient at the maximum equal to 5 cm^{-1}. This means that, by using conventional pumping at 801 nm, it is difficult to provide spatially

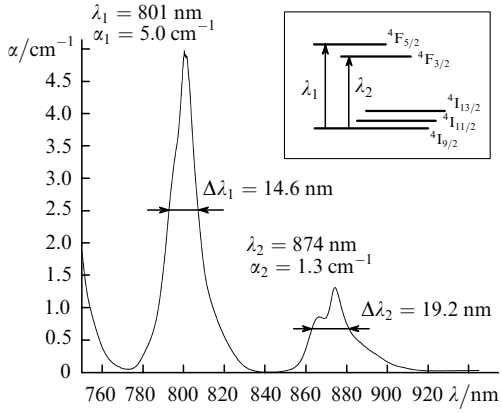

Figure 2. Absorption spectrum of the active element. The positions and widths of the bands and maximum absorption coefficients are indicted. The inset shows the diagram of several levels of the Nd^{3+} ion.

homogeneous excitation of the active medium thicker than 1 cm. Of course, we do not consider here excitation into the wings of the absorption line because in this case the pump efficiency strongly depends on the pump radiation spectrum. In addition, the wings of the absorption line correspond to ions that are located in the environment that drastically differs from that of other ions in a glass matrix. The rate of nonradiative relaxation for these ions can be higher than that for others.

Figure 3 shows the luminescence spectrum $I(\lambda)$ of the GLS-22 sample excited by a diode array at 800 nm. The wavelengths λ_i of the luminescence bands and their effective widths $\Delta\lambda_i$ and the relative probabilities w_i of transitions from the upper level to the levels $^4I_{9/2}$, $^4I_{11/2}$, and $^4I_{13/2}$ presented in the figure were found from the expressions

$$w_i = \frac{A_i}{A_1}, \quad A_i = \lambda_i \Phi_i,$$

$$\Phi_i = \int I_i(\lambda)\mathrm{d}\lambda, \quad \Delta\lambda_i = \frac{\Phi_i}{I(\lambda_i)}, \quad i = 1, 2, 3 \qquad (1)$$

similar to those used in [14]. The values of w_1, w_2, and w_3 obtained in this way and equal to 1, 1.29, and 0.22, respectively, are close to those used conventionally in the literature for the GLS-22 glass. In particular, handbook [15] gives the values 1, 1.5, and 0.27.

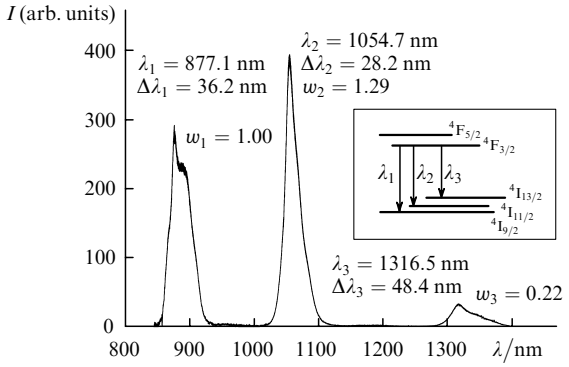

Figure 3. Luminescence spectrum of the active sample excited by a diode array at $\lambda \approx 800$ nm. The positions and widths of the bands and the probabilities of the corresponding transitions are indicated. The inset shows the diagram of several levels of the Nd^{3+} ion.

Another important parameter of the active element is the lifetime τ of the upper excited $^4F_{3/2}$ level. It was measured from the luminescence decay at a wavelength of 1055 nm shown in Fig. 4. The digital processing of the decay curve showed that the luminescence decay by an order of magnitude occurs exponentially with the decay time $\tau =$ 280 μs (with an accuracy better than 2 %).

These data allow us to calculate the cross section for the stimulated transition at the maximum of the 1055-nm band. By using the well-known relation, we find that

$$\sigma = \frac{\eta\lambda_2^4}{8\pi\tau c n^2 \Delta\lambda_2} \frac{w_2}{w_1 + w_2 + w_3}, \qquad (2)$$

where η is the total quantum yield of luminescence for the three bands shown in Fig. 3; n is the refractive index for $\lambda_2 = 1055$ nm; and c is the speed of light. By substituting the found values of parameters into (2), we obtain

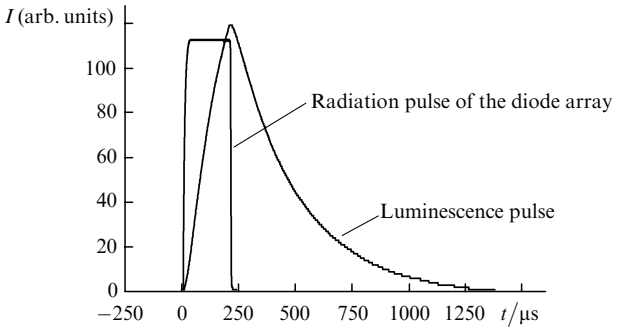

Figure 4. Time dependences of the 800-nm pump intensity and luminescence of the active element at 1055 nm.

$$\sigma = \eta\, 3.86 \times 10^{-20}\ \mathrm{cm}^2. \qquad (3)$$

The value of the cross section for this glass used in the literature (see, for example, [16]) is $\sigma \sim (3.2 \pm 0.4) \times 10^{-20}$ cm^2. For this value of σ, the quantum yield is $\eta \approx 0.83 \pm 0.10$.

2.3 Radiation of diode arrays and optical amplification in the active element

Figure 5 presents the light–current characteristic of the diode array operating in the repetitively pulsed regime. The insets show the pulse shape and emission spectrum averaged over the pulse duration. Heterolasers are somewhat heated during the radiation pulse, resulting in the red shift of the emission spectrum of the diode array. This is demonstrated in Fig. 6 presenting the shapes of radiation pulses from the diode array at different wavelengths and the emission spectra recorded at different instants.

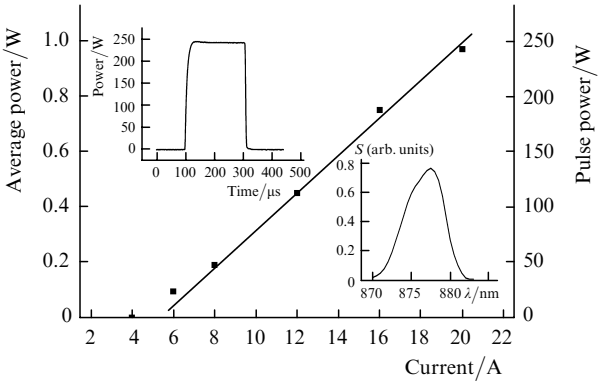

Figure 5. Dependence of the output power of the diode array on the pump current. The inset at the top shows the radiation pulse of the array integrated over the spectrum, at the bottom – the integrated (averaged over the pulse duration) emission spectrum of the diode array.

The radiation patterns of diode arrays for mutually perpendicular directions are presented in Fig. 7. As mentioned above, the divergence in the plane of the p–n junction of heterolasers proves to be most critical for this pump scheme. The angle of the radiation pattern corresponding to the frustrated total internal reflection was 17° in our case (from the radiation-pattern centre). This angle is indicated by the arrow in Fig. 7a. One can see that only a small part of the optical-beam energy (less than 1 %) is emitted at angles exceeding 17°.

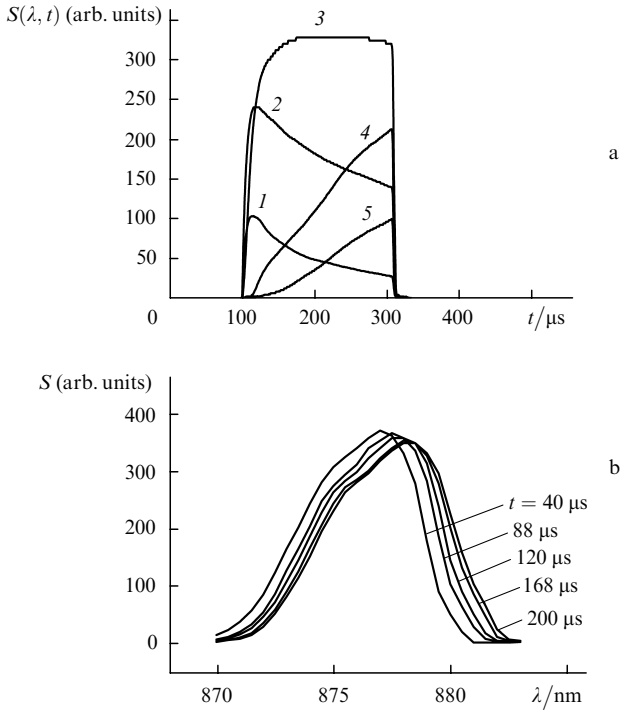

Figure 6. Time dependences of the radiation intensity of the diode array with a narrow spectral band (~0.5 nm) at $\lambda = 874$ (*1*), 876 (*2*), 878 (*3*), 880 (*4*), and 881 nm (*5*) and the emission spectra of the diode array at different instants t from the pulse onset (b).

The results of the measurements described above allow us to calculate the pump efficiency μ, i.e., the fraction of radiation energy of diode arrays transformed to the excitation energy of ions by the end of the pump pulse:

$$\mu = \mu_q \mu_g \mu_s \mu_T, \tag{4}$$

where $\mu_q = \lambda_p/\lambda_L$ is the ratio of the pump wavelength to the laser wavelength (the so-called pump quantum defect, which is 0.82 in our case); μ_g is the geometrical factor equal to the fraction of radiation energy of diode arrays pumped into the active element; μ_s is the spectral factor equal to the fraction of energy absorbed by the active element; μ_T is the fraction of absorbed energy that preserved as the excitation energy of Nd^{3+} ions by the end of the pump pulse.

The value of μ_g is smaller than unity due to the losses of radiation coupled to the prism (Fig. 1b) and the escape of radiation from the active element beyond the total internal reflection angle ($\theta > 17^\circ$). Under our experimental conditions, this value was $\mu_g \simeq 0.89$.

The spectral factor μ_s was found from the relation

$$\mu_s = \int \{1 - \exp[-\alpha(\lambda)l]\} S(\lambda) d\lambda \left[\int S(\lambda) d\lambda\right]^{-1}, \tag{5}$$

where $S(\lambda)$ is the average (over the pulse duration) spectral density of the radiation intensity of the diode array (the lower inset in Fig. 5); $\alpha(\lambda)$ is the absorption coefficient in the 874-nm band (Fig. 2); and l is the length of the pumped region. In our case (Fig. 1a), the length l was determined by the distance between the adjacent prisms taking into account the inclined propagation of the beam and was ~6 cm. The spectral factor μ_s calculated from (5) by using the obtained spectral data was 0.98. The difference of μ_T from unity is caused by the finite lifetime $\tau = 280$ μs of excited Nd^{3+} ions. For a rectangular pump pulse of duration T, as in our experiment, we have

$$\mu_T = \frac{\tau}{T}\left[1 - \exp\left(-\frac{T}{\tau}\right)\right]. \tag{6}$$

For the pulse duration $T = 200$ μs, we obtain $\mu_T = 0.71$. Thus, according to (4), we finally have $\mu = 0.51$.

To measure the optical gain, the probe semiconductor laser was thermally stabilised at the temperature 5–10° below room temperature. The temperature was selected to make the maximum of the emission spectrum of the probe laser coincident with that of the luminescence spectrum of the laser transition. The average gain was found by processing the data obtained from oscillograms of the probe beam intensity transmitted through the rod:

$$g = \frac{1}{L}\ln\frac{I_{max}}{I_0}, \tag{7}$$

where L is the total length of the rod; I_{max} is the probe-beam intensity at the end of the pump pulse; and I_0 is the intensity at the instant immediately before the pump pulse. Figure 8 presents the measured values of g. The insets in this figure show the oscillogram of the probe-beam intensity transmitted through the active element (at the top) and the luminescence spectrum of the active element and the emission spectrum of the probe laser (at the bottom). The value of g was measured as a function of the average specific accumulated pump energy p defined by the relation

$$p = \frac{\mu E}{V}, \tag{8}$$

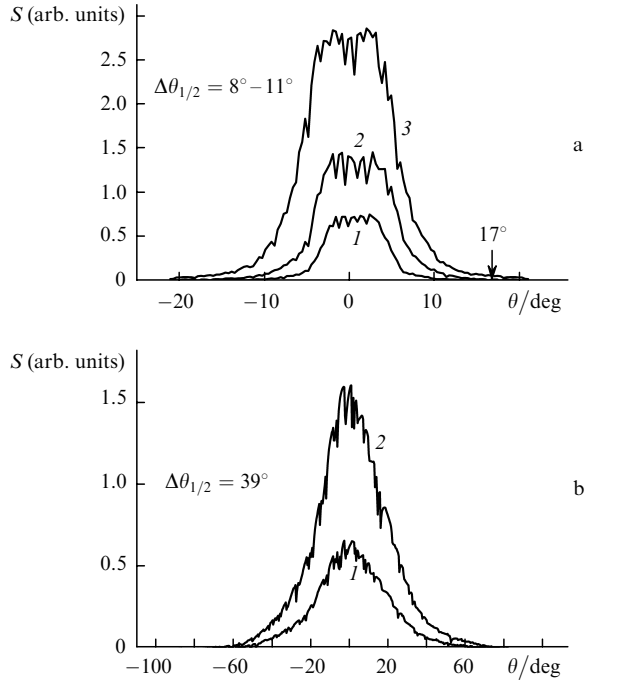

Figure 7. Radiation patterns of diode arrays for pump currents 8 (*1*), 12 (*2*), and 20 A (*3*): intensity distribution along the 'slow' (in the p–n junction plane) (a) and 'fast' (in the plane perpendicular to the structure layers) (b) axes. The arrow in Fig. 7a indicates the angle of the radiation pattern corresponding to the frustrated total internal reflection.

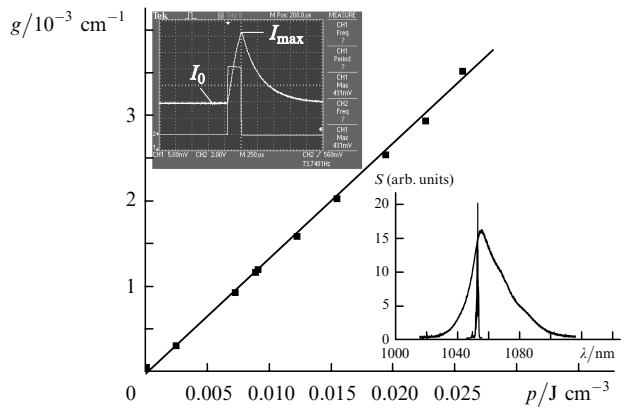

Figure 8. Dependence of the gain on the pump energy density stored in the active element. The inset at the top shows the oscillograms of the probe-laser pulse and pump current pulse; at the bottom – the luminescence spectrum of the sample and probe laser radiation.

where $E = 4PT$ is the pulse energy emitted by four diode arrays; P is the pulsed radiation power of one diode array; V is the total volume of the active element (in our case $V = 6.7$ cm^3). The maximum value of g obtained in our paper was $\sim 3.5 \times 10^{-3}$ cm^{-1}. The slope of the dependence of g on p gives the specific gain equal to 1.33×10^{-1} cm^2 J^{-1}. This value (in the case of uniform pumping or for the spatially averaged gain and density of the stored pump energy) should be equal to the ratio of the cross section to the probe laser photon energy $\hbar\omega$, which allows us to find the cross section σ from Fig. 8. This cross section was 2.75×10^{-20} cm^2. Here, we used the small-gain condition

$$g_{\max} \frac{L}{4} < 1, \tag{9}$$

where $g_{\max}$ is the maximum local value of the gain inside the active element. By comparing the found value of σ with expression (3), we obtain the quantum yield $\eta = 0.71$. By using this value of η and the spectral characteristics of the $^4F_{3/2} - {}^4I_{9/2}$ band, we can find from (2) the cross section for this band as well. It was 7.7×10^{-21} cm^2. According to Fig. 2, the absorption coefficient at the maximum of this band is 1.3 cm^{-1}. This gives the concentration N of Nd^{3+} ions in our sample:

$$N = \frac{\alpha(\lambda = 874 \text{ nm})}{\sigma(\lambda = 877 \text{ nm})} = 1.7 \times 10^{20} \text{ cm}^{-3}. \tag{10}$$

The concentration for glasses of this type reported in the literature is 2×10^{20} cm^{-3}, which demonstrates the acceptable accuracy of the parameters of our sample for using them in simulations of laser systems.

3. Discussion and conclusions

Note that resonance pumping used in our paper is promising mainly only for high-power laser systems. For low-power lasers, it is worthwhile to reduce the active-medium volume for increasing the pump energy density. It is obvious that this requires a small length at which a considerable fraction of the pump radiation is absorbed. In this case, conventional pumping at the 800-nm $^4I_{9/2} - {}^4F_{5/2}$ transition, where absorption is four times stronger than in the 870-nm band, proves to be more advantageous to minimise the threshold pump power.

It is for this reason that resonance pumping was almost not used in earlier papers and its application in high-power lasers was reported only in the last years. Indeed, when large volumes of the active medium are required (this is necessary in high-power lasers to reduce the specific thermal load and decrease the laser radiation density), a small absorption length is not an advantage but a disadvantage because it results in a spatially nonuniform excitation of the active medium.

It is obvious that the pump efficiency ~ 0.5 achieved in the paper is not ultimate. It can be increased, first, by varying the geometrical factor μ_g, which can exceed 0.9 in the optimised pump system, and, second, by increasing the factor μ_T determined by the ratio τ/T. The increase can be achieved both by decreasing T, for example, down to 100 μs and by increasing τ. The first is related to the increase in the radiation resistance of the output mirrors of heterolasers in the diode array and to the increase in the pump beam brightness due to the use of diode arrays with internal lenses providing a decrease in the divergence along the 'fast' axis. This will allow one to increase the pump intensity, thereby decreasing by the same factor the pulse duration for the same energy. The value of τ can be increased only by selecting a proper material (a phosphate glass in our case). It seems that this can be done by improving the glass quality by decreasing the rate of nonradiative relaxation in it. Indeed, the quantum yield $\eta = 0.71$ is not high for the concentration of Nd^{3+} ions equal to 2×10^{20} cm^{-3}. An increase in η automatically means an increase in τ. The value $\tau \approx 320$ μs for the phosphate glass can be readily obtained. Of course, a drastic increase in τ can be achieved only in other active media, for example, doped with Yb ions.

Although the gains $\sim 3.5 \times 10^{-3}$ cm^{-1} at the laser transition achieved at present are acceptable for lasing, they are not optimal from the point of view of the efficiency of a high-power laser. It is obvious that this value can be increased by several times (up to an order of magnitude) by increasing the pump energy density. In our paper, this density was limited by the number of diode arrays available. Our experiments and estimates show that no thermal-regime limitations appear in the active element if cooled with gaseous helium rather than by air. The gains of $3 \times 10^{-2} - 5 \times 10^{-2}$ cm^{-1} are already quite sufficient for active elements of length of the order of a few tens of centimetres, which is typical for high-power lasers.

Of course, the necessary condition for realisation of high radiative characteristics of lasers at such gains in the medium is rather strict requirements to the upper limit of inactive absorption of the material at the laser wavelength. Our estimates show that to obtain the lasing efficiency $\sim 60\,\%$ with respect to the pump energy for the gain of the medium 3×10^{-2} cm^{-1}, the losses in the active element should not exceed 0.7×10^{-3} cm^{-1}. Although this is a serious requirement to the glass quality, it can be fulfilled at present. The absorption coefficient at the laser wavelength for the glass under study was $\sim 5 \times 10^{-3}$ cm^{-1}, which prevented lasing in our case.

Therefore, we can make the following conclusions based on the results of our study:

(i) We performed for the first time the resonance pumping of a Nd-doped phosphate glass by radiation from diode arrays and achieved the gain 3.5×10^{-3} cm^{-1};

(ii) the pump efficiency for a glass sample of volume 6.7 cm^3 was 0.51;

(iii) the specific gain, pump efficiency, and quantum yield were found under conditions that were most close to those for high-power lasers, when the thickness of the pumped region is several centimetres for the high degree of integration of diode sources. This opens up the possibility for reliable simulations of such systems based on the data obtained.

The methods developed in our paper can be also considered as the way to test active media intended for high-power lasers. Based on our results, we can conclude that one of the basic criteria of the quality of the optical glass used for diode pumping is the high quantum yield (increased τ) and the low absorption coefficient at the laser wavelength.

Acknowledgements. The authors thank V.G. Shutyak for the fabrication of the active element of the original design. This work was partially supported by the program 'Coherent optical radiation of semiconductor compounds and structures' of the Department of Physical Sciences of RAS.

References

1. Kravtsov N.V. *Kvantovaya Elektron.*, **31**, 661 (2001) [*Quantum Electron.*, **31**, 661 (2001)].
2. Orth C.D., Payne S.A., Krupke W.F. *Nuclear Fusion*, **36**, 75 (1996).
3. Bruesselbach H., Sumida D.S. *IEEE J. Sel. Top. Quantum Electron.*, **11**, 600 (2005).
4. Hai-Feng L. et al. *Chin. Phys. Lett.*, **22**, 2565 (2005).
5. Krupke W.F. *IEEE J. Sel. Top. Quantum Electron.*, **6**, 1287 (2000).
6. Pierre E.J.S. *IEEE J. Sel. Top. Quantum Electron.*, **3**, 53 (1997).
7. Kurita T. et al. *Techn. Dig. Conf. «Lasers and Electrotechnol. 2005»* (Washington, DC: OSA, 2005) CMJ5.
8. Hein J. et al. *Appl. Phys. B*, **79**, 419 (2004).
9. Schleuter H., Schnitzler C. *Techn. Dig. «Conf. Lasers and Electrotechnol. 2005»* (Washington, DC: OSA, 2005) PWC2.
10. Lupei V., Pavel N. *Opt. Lett.*, **26** (21), 1678 (2001).
11. Lupei V., Pavel N., Taira T. *IEEE J. Sel. Top. Quantum Electron.*, **38**, 240 (2002).
12. Saikawa J., Sato Y., Taira T., Nakamura O., Furukawa Y.C. *Techn. Dig. Conf. «Lasers and Electrotechnol. 2005»* (Washington, DC: OSA, 2005) CMS6.
13. Alimov O.K., Basiev T.T., Mirov S.B. *Trudy IOFAN*, **9**, 6 (1987).
14. Dianov E.M., Karasik A.Ya., Kut'enkov A.A., Neustruev V.B., Shcherbakov I.A. *Kvantovaya Elektron.*, **3**, 168 (1976) [*Sov. J. Quantum Electron.*, **6**, 90 (1976)].
15. Buzhinskii I.M., Dianov E.M., Mak A.A. *Promyshlennye lazernye stekla. Spravochnik po lazeram. T. 1* (Commercial Laser Glasses. Handbook on Lasers, Vol. 1) (Moscow: Sov. Radio, 1978).
16. Mak A.A., Soms L.N., Fromzel' V.A., Yashin V.E. *Lazery na neodimovom stekle* (Neodymium Glass Lasers) (Moscow: Nauka, 1990).